Zinc- and pH-Dependent Conformational Transition in a Putative Interdomain Linker Region of the Influenza Virus Matrix Protein M1[†]

Atsushi Okada, Takashi Miura, and Hideo Takeuchi*

Graduate School of Pharmaceutical Sciences, Tohoku University, Aobayama, Sendai 980-8578, Japan

Received November 14, 2002; Revised Manuscript Received January 7, 2003

ABSTRACT: The matrix protein M1 of influenza A virus forms a shell beneath the viral envelope and sustains the virion architecture by interacting with other viral components. A structural change of M1 upon acidification of the virion interior in an early stage of virus infection is considered to be a key step to virus uncoating. We examined the structure of a 28-mer peptide (M1Lnk) representing a putative linker region between the N- and C-terminal domains of M1 by using circular dichroism, Raman, and absorption spectroscopy. M1Lnk assumes an α-helical structure in a mildly hydrophobic environment irrespective of pH, being consistent with the X-ray crystal structures of an N-terminal fragment of M1 at pH 7 and 4. In the presence of Zn^{2+}, on the other hand, M1Lnk takes a partially unfolded conformation at neutral pH with a tetrahedral coordination of two Cys residues and two His residues to a Zn^{2+} ion in the central part of the peptide. Upon acidification, the peptide releases the Zn^{2+} ion and refolds into the α-helix-rich structure with a midpoint of transition at pH 5.9. The pH-dependent conformational transition of M1Lnk strongly suggests that the interdomain linker region of M1 also undergoes a pH-dependent unfolding−refolding transition in the presence of Zn^{2+}. A small but significant portion of the M1 protein is bound to Zn^{2+} in the virion, and the Zn^{2+}-bound M1 molecule may play a special role in virus uncoating by changing the disposition of the N- and C-terminal domains upon acidification of the virion interior.

The matrix protein M1 of influenza A virus is the most abundant viral component, and about three thousand copies of M1 form a shell surrounding eight ribonucleoprotein (RNP)[1] cores (*1*−*4*). The outer surface of the M1 shell is covered with a lipid membrane envelope, which carries the transmembrane channel protein M2 and two membrane-anchored external glycoproteins, hemagglutinin (HA) and neuraminidase (NA). The architecture of the virion is stabilized by interactions of M1 with the RNP cores, lipid membrane, and cytoplasmic tails of HA and NA as well as with adjacent M1 molecules in the shell (*5*−*9*). In addition to being a major structural component, the M1 protein plays a crucial role in virus replication. Upon infection to a host cell, the virion is internalized by HA-mediated endocytosis, and the ion channel M2 protein opens to allow proton flux from the acidic endosomal compartment into the virion (*10*−*13*). The acidified virion interior (pH ∼5) induces dissociation of M1 from RNP and other structural components, leading to virus uncoating (*14*−*16*). Later in the virus replication cycle, the M1 protein transports newly synthesized RNP cores from the nucleus to the cytoplasm and promotes the assembly of virion components for budding at the host cell membrane (*17*−*22*). A pH-dependent structural change of M1 is considered to be a key factor that regulates the interactions of M1 with other viral components (*14*−*16*).

The intact M1 protein is composed of 252 amino acid residues (*23*, *24*). However, the crystals examined by X-ray diffraction contained only the N-terminal fragment up to Gln164 because of proteolytic cleavage during the crystallization (*25*−*27*). In the crystal structure, the N-terminal fragment folds into a globular domain composed of two subdomains, each of which consists of four α-helices. The domain structure of the N-terminal fragment is identical between the crystals prepared at pH 7 and 4, and the influence of pH is seen only in the crystal packing (*25*−*27*). The structure of the full-length M1 protein has been studied in solution by circular dichroism (CD), small angle neutron scattering, and tritium bombardment (*26*, *28*). All of the solution experiments have suggested that the C-terminal region (residues 165−252), which was not analyzed by X-ray diffraction, also forms a domain rich in α-helical structure at both neutral and acidic pH. These observations raise the possibility that a pH-dependent structural change of M1 occurs in the linker region between the N- and C-terminal domains rather than within the domains themselves. Residues 159−164 (His[159]-Arg-Ser-His-Arg-Gln[164]) at the C-terminal tail of the N-terminal fragment are disordered in the crystal structure and considered to be part of the interdomain linker region (*25*, *26*). The putative linker region contains His159 and His162, and protonation of the His imidazole rings might be the origin of the expected pH sensitivity of the M1 structure. Another structural characteristic of the putative linker region is the presence of a highly conserved Zn finger-like Cys_2His_2 motif, Cys[148]-Cys[151]-

[†] This work was supported in part by a Grant-in-Aid (No. 11440169) from the Ministry of Education, Science, Sports, and Culture of Japan.

* Corresponding author. Phone/Fax: +81-22-217-6855. E-mail: takeuchi@mail.cc.tohoku.ac.jp.

[1] Abbreviations: CD, circular dichroism; DTT, dithiothreitol; HA, hemagglutinin; HEPES, *N*-(2-hydroxyethyl)piperazine-*N*′-2-ethanesulfonic acid; M1Lnk, a 28-residue peptide representing the putative linker region of M1; NA, neuraminidase; MES, 2-(*N*-morpholino)-ethanesulfonic acid; RNP, ribonucleoprotein; TFE, trifluoroethanol.

10.1021/bi027176t CCC: $25.00
Published on Web 01/30/2003

His[159]-His[162], which actually binds a Zn^{2+} ion in vitro and in vivo (*5*, *29*, *30*), though the crystals examined by X-ray diffraction did not contain Zn^{2+} ions (*25*, *26*).

In this study, we have examined the effects of pH and Zn^{2+} binding on the structure of a 28 amino acid peptide that represents the putative linker region including the Cys_2His_2 motif: Ac-Thr[139]-Thr-Glu-Val-Ala-Phe-Gly-Leu-Val-Cys[148]-Ala-Thr-Cys[151]-Glu-Gln-Ile-Ala-Asp-Ser-Gln-His[159]-Arg-Ser-His[162]-Arg-Gln-Met-Val[166]-amide (M1Lnk). Analyses of absorption, CD, and Raman spectra have shown that Zn^{2+}-free M1Lnk takes an α-helical structure irrespective of pH. In the presence of Zn^{2+}, however, the peptide exhibits a strong pH dependence. At neutral pH, a Zn^{2+} ion binds to the Cys_2His_2 motif and induces a partially unfolded structure, whereas the peptide retains the α-helical structure at acidic pH without binding to Zn^{2+}. The pH-dependent conformational transition of M1Lnk in the presence of Zn^{2+} strongly suggests that the interdomain linker region of Zn^{2+}-bound M1 also undergoes a conformational transition from partially unfolded to α-helical upon acidification of the virion interior.

EXPERIMENTAL PROCEDURES

Peptide Synthesis and Purification. The peptide M1Lnk, whose amino acid sequence was taken from human influenza virus A/PR/8/34 (*23*, *24*), was synthesized on an Applied Biosystems Model 431A automated peptide synthesizer by using amino acid derivatives protected by the 9-fluorenylmethoxycarbonyl group. The N- and C-termini of the peptide were acetylated and amidated, respectively, on the peptide synthesizer. The peptide was cleaved from the resin, purified by HPLC on a reversed-phase column, and lyophilized as the hydrochloride salt. The disulfide linkages formed by autoxidation of Cys were reduced by incubation with dithiothreithol (DTT) for 40 min at 60 °C. DTT and its oxidation products were removed by HPLC on a gel-filtration column. All sample manipulations after the reduction were performed under an atmosphere of high-purity argon. The concentration of M1Lnk in stock solution was determined from the intensity of the 1003 cm^{-1} band of Phe144 relative to that of the 933 cm^{-1} band of ClO_4^- added as an internal intensity standard. A Jasco NR-1800 visible Raman spectrometer was used for the concentration determination.

Acquisition of Spectral Data. CD spectra were recorded on a Jasco J-720 polarimeter using a 1 mm quartz cell. M1Lnk was dissolved at a concentration of 25 μM in 1 mM buffer of *N*-(2-hydroxyethyl)piperazine-*N*′-2-ethanesulfonic acid (HEPES, pH 6.5−8) or 2-(*N*-morpholino)ethanesulfonic acid (MES, pH 4.5−6.5) containing 100 mM $NaClO_4$ and 0−50% (v/v) 2,2,2-trifluoroethanol (TFE). When the effect of Zn^{2+} binding was examined, 1 equiv of $ZnCl_2$ was added to the solution. The samples of different solution conditions were prepared separately, and the CD spectrum of each sample was recorded twice to ensure equilibration. The recorded CD intensity was converted into molar ellipticity [θ] per residue. Estimation of the secondary structure content from CD spectra was performed with the software CDNN based on a neural network algorithm (*31*).

Absorption spectra were recorded on a Hitachi U-3300 spectrophotometer using a 1 cm quartz cell. Titration of M1Lnk with metal ions was performed by adding aliquots of a 5 mM aqueous solution of $ZnCl_2$ or $CoCl_2$ to a 2 mL solution of M1Lnk (25 μM peptide, 30 mM HEPES, 100 mM $NaClO_4$, pH 7.4) in the presence and absence of 50% (v/v) TFE. Identical results were obtained in two independent titration experiments.

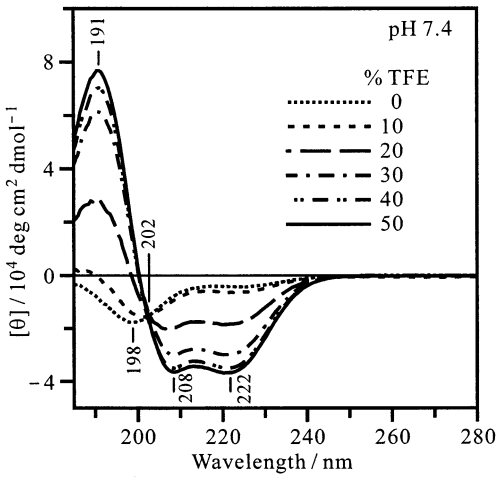

FIGURE 1: CD spectra of M1Lnk in neat aqueous solution (dotted line) and in 10−50% (v/v) TFE solution. The solutions contained 25 μM peptide, 1 mM HEPES (pH 7.4), and 100 mM $NaClO_4$. The corresponding CD spectra at pH 5.4 were almost identical to the spectra shown here.

UV Raman spectra were excited with 244 nm continuous wave radiation from an intracavity frequency-doubled argon ion laser (Coherent Innova 300 FReD) and recorded on a UV Raman spectrometer (Jasco TR-600UV) equipped with a UV-enhanced CCD detector (Princeton Instruments LN/CCD-1752). The sample solution was stirred with a magnetic stirrer in a quartz optical cell of 2 mm path length. The concentration of M1Lnk was 0.8 mM in 30 mM HEPES (pH 7.4) or MES (pH 5.4) buffer containing 100 mM $NaClO_4$ and 50% (v/v) TFE. One equivalent of $ZnCl_2$ was added to the peptide solution for preparation of the Zn^{2+}−M1Lnk complex. Raman signals of each sample were accumulated for 45 min, and the spectra of two fresh samples were summed to improve the signal-to-noise ratio. The Raman spectra were highly reproducible, and no photochemical degradation of the sample was detected.

RESULTS

Secondary Structure of M1Lnk. Figure 1 shows the CD spectra of M1Lnk at pH 7.4 in the absence of Zn^{2+}. In aqueous solution, M1Lnk gives a negative weak peak at 198 nm, indicating that the peptide mostly assumes irregular structure (*32*). This is in sharp contrast to the highly helical structure found in the crystal of the N-terminal fragment (*26*, *27*). In the crystal, two-thirds (from Thr140 to Gln158) of the putative linker region forms an α-helix named H9. The difference in secondary structure between the N-terminal fragment and M1Lnk may be attributed to a difference in environment of the peptide chain. Actually, most of helix H9 is surrounded by hydrophobic side chains extruding from the other four helices, H1, H4, H7, and H8, in the crystal of M1 (*26*, *27*), whereas the environment of the M1Lnk peptide in aqueous solution is hydrophilic.

To elevate the environmental hydrophobicity, we added TFE to the aqueous solution of M1Lnk. TFE is known to stabilize α-helices in regions with α-helical propensity of

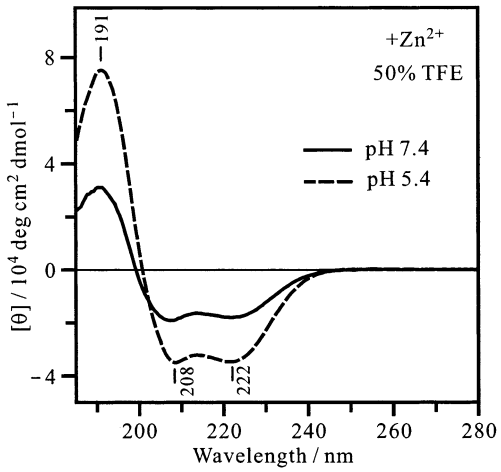

FIGURE 2: CD spectra of M1Lnk in the presence of equimolar Zn^{2+} at pH 7.4 and 5.4. The solution contained 25 μM peptide, 25 μM $ZnCl_2$, 1 mM HEPES (pH 7.4) or MES (pH 5.4), 100 mM $NaClO_4$, and 50% (v/v) TFE. The effect of Zn^{2+} may be seen by comparing these spectra with the spectrum in 50% (v/v) TFE solution (solid line) in Figure 1.

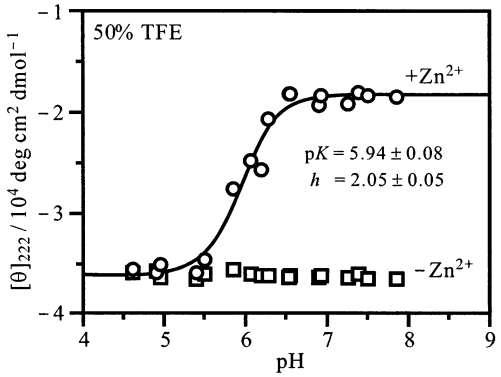

FIGURE 3: Mean residue ellipticity at 222 nm ($[\theta]_{222}$) of M1Lnk plotted as a function of pH in the absence (squares) and presence (circles) of Zn^{2+}. The ellipticity was recorded for solutions containing 25 μM peptide, 1 mM HEPES (pH 6.5−8) or MES (pH 4.5−6.5), 100 mM $NaClO_4$, and 50% (v/v) TFE. One equivalent of Zn^{2+} was added when necessary. The curve shows a fit with a Hill equation.

peptides and proteins (*33*, *34*). With increase of the TFE content, the negative ellipticity at 222 nm characteristic of the α-helical structure (*32*) gradually increases in magnitude and becomes saturated at 50% TFE (Figure 1). We also examined the effect of TFE at pH 5.4. The CD spectra recorded at pH 5.4 were identical to those at pH 7.4 (data not shown), indicating that the secondary structure of M1Lnk is insensitive to pH as expected from the identical X-ray crystal structure at pH 7 and 4 (*25*−*27*).

The CD spectra in 0−50% TFE solutions exhibit an isodichroic point at 202 nm (Figure 1), which provides evidence that the transition involves only two discrete conformational states. Deconvolution of the CD spectra with the software CDNN indicates that the α-helical content is about 10% in the absence of TFE and about 90% at 50% TFE. The M1Lnk conformation can be either irregular or α-helical without any intermediate conformation. The α-helical content of M1Lnk in 50% TFE solution is higher than that (68%) expected from the crystal structure of the N-terminal fragment, suggesting that the region adjacent to H9, His^{159}-Arg-Ser-His-Arg-Gln-Met-Val^{166}, also has α-helical propensity. It is likely that helix H9 somewhat extends to the C-terminal side under the moderately hydrophobic environment of 50% TFE solution. Although there is a small difference in the extent of α-helical structure, the conformation of M1Lnk in 50% TFE solution may be regarded as representing the conformation of the putative linker region of M1, at least in the major H9 region that covers two-thirds of the Cys_2His_2 motif and includes both Cys residues.

Effect of Zn^{2+} on the Secondary Structure of M1Lnk. Since M1Lnk contains a Cys_2His_2-type Zn^{2+}-binding motif in the central part of the peptide chain, we have examined the effect of Zn^{2+} on the conformation of M1Lnk in 50% TFE solution. Figure 2 shows the CD spectrum of M1Lnk at pH 7.4 in the presence of 1 equiv of Zn^{2+} (solid line). Compared to the CD spectrum in the absence of Zn^{2+} (Figure 1, solid line), the negative CD peak at 222 nm is decreased to about half in depth and a larger intensity loss is seen for the positive peak at 191 nm. Analysis of the CD spectral change with the CDNN program indicates that the α-helical content is reduced to about 50%, and instead random coil and β-turn structures are generated in Zn^{2+}-bound M1Lnk. The binding of Zn^{2+} at pH 7.4 induces helix unfolding in about half of the region of the M1Lnk peptide chain. In sharp contrast, addition of Zn^{2+} at pH 5.4 has little effect. The CD spectrum recorded at pH 5.4 in the presence of Zn^{2+} (Figure 2, broken line) is almost identical to that in the absence of Zn^{2+} (Figure 1, solid line). M1Lnk retains the α-helical structure at pH 5.4 even in the presence of Zn^{2+}, suggesting that no Zn^{2+}−peptide interaction takes place at acidic pH.

pH Dependence of the M1Lnk Secondary Structure. The CD spectral data described above suggest that the interaction between Zn^{2+} and M1Lnk critically depends on pH. We have examined the pH dependence of the M1Lnk conformation in the presence of Zn^{2+} by recording CD spectra at varied pH. Since the sample solutions at different pH values were prepared separately as described in the Experimental Procedures, any pH dependence, if observed, may be regarded reversible. Figure 3 shows the ellipticity at 222 nm, $[\theta]_{222}$, a measure of the α-helical content, plotted as a function of pH in a range from 4.5 to 8. The ellipticity measurements were made in the absence and presence of Zn^{2+} in 50% TFE solution. In the absence of Zn^{2+}, $[\theta]_{222}$ is nearly constant at -3.6×10^4 deg cm^2 dmol^{-1} over the pH range examined, indicating that M1Lnk remains highly α-helical irrespective of pH. On the other hand, the $[\theta]_{222}$ value in the presence of 1 equiv of Zn^{2+} shows a sigmoidal change between -3.6×10^4 and -1.8×10^4 deg cm^2 dmol^{-1} with a midpoint of transition around pH 6 (Figure 3). Analysis of the pH dependence with a Hill equation yields $pK = 5.94 \pm 0.08$ for the proton binding constant and $h = 2.05 \pm 0.05$ for the Hill coefficient (*35*, *36*). The value of the Hill coefficient suggests that the transition between the highly α-helical state at acidic pH and the partially unfolded state at neutral pH is a cooperative process involving two protonation sites. Since the pK value is close to the pK_a value (∼6.5) of the imidazole ring of His, the pH-dependent conformational transition of M1Lnk in the presence of Zn^{2+} may be related to protonation of two His residues, His159 and His162.

Zn^{2+}-Binding Sites of M1Lnk. To elucidate the Zn^{2+}-binding sites of M1Lnk, we have examined UV (244 nm) Raman spectra of 50% TFE solutions of M1Lnk at pH 7.4 and 5.4 in the absence and presence of Zn^{2+}. Figure 4 shows

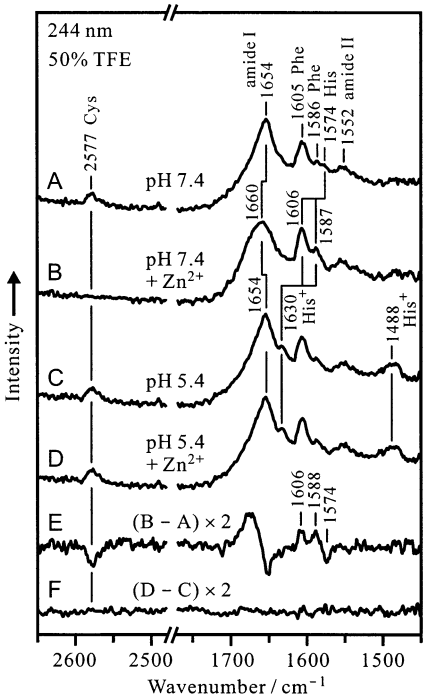

FIGURE 4: UV (244 nm) Raman spectra of M1Lnk at (A, B) pH 7.4 and (C, D) pH 5.4 in the (A, C) absence and (B, D) presence of Zn^{2+}. Traces D and E show the difference spectra (B) − (A) and (D) − (C), respectively. The solutions contained 0.8 mM peptide, 30 mM HEPES (pH 7.4) or MES (pH 5.4), 100 mM $NaClO_4$, and 50% (v/v) TFE. One equivalent of Zn^{2+} was added when necessary.

the Raman spectra in the 2650−2500 and 1750−1450 cm^{-1} regions, where there are expected Raman bands of His and Cys side chains as well as the peptide main chain. The strongest Raman band at 1654 cm^{-1} in the spectrum of Zn^{2+}-free M1Lnk at pH 7.4 (Figure 4A) is assigned to the amide I vibration, and its wavenumber indicates that the peptide is in α-helical structure (*37*), being consistent with the CD spectra reported above. A weak Raman band at 1574 cm^{-1} is ascribed to the C_4═C_5 stretch of His in the neutral imidazole form (*38*, *39*). The 2577 cm^{-1} band is assigned to the S−H stretch of Cys hydrogen bonded with a weak proton acceptor or a donor/acceptor (*40*). The relative intensity of the Cys and His Raman bands in Figure 4A corresponds well with that observed for an equimolar mixture of amino acids Cys and His dissolved in the same solvent (spectrum not shown), giving support for the assignments of the 2577 and 1574 cm^{-1} Raman bands.

Upon addition of Zn^{2+} at pH 7.4, the Raman spectrum changes in some wavenumber regions (Figure 4B). The spectral changes are more clearly seen in the difference spectrum, (B) − (A) (Figure 4E). The amide I band shifts from 1654 to 1660 cm^{-1}, reflecting the partial unfolding of the helix revealed by CD spectroscopy. The 1574 cm^{-1} His Raman band disappears, and instead two weak bands appear at 1606 and 1587 cm^{-1} (the 1606 cm^{-1} band is overlapped by the stronger Phe band at the same wavenumber). According to the relationships between the C_4═C_5 stretch wavenumber and metal coordination (*38*, *39*), the newly generated Raman bands at 1606 and 1587 cm^{-1} are assigned to His residues coordinating to Zn^{2+} via the N_τ and N_π atoms, respectively, of the imidazole ring. One of His159 and His162 must be bound to a Zn^{2+} ion via the N_τ atom and the other via the N_π atom. The disappearance of the 1574 cm^{-1} band gives evidence for the absence of metal-free His residues. The S−H stretch band of Cys at 2577 cm^{-1} also disappears, indicating that both Cys148 and Cys151 are bound to Zn^{2+}. It is evident that Cys148, Cys151, His159, and His162 are all ligated to Zn^{2+}.

At pH 5.4 (Figure 4C), two new Raman bands appear at 1630 and 1488 cm^{-1}, which are assigned to the protonated imidazolium ring of His (*41*). The S−H stretch band of Cys is also seen at pH 5.4. The prominent α-helical amide I band at 1654 cm^{-1} supports the high α-helical content indicated by the CD spectrum. The Raman spectrum of M1Lnk in the presence of Zn^{2+} (Figure 4D) is almost identical to that in the absence of Zn^{2+} (Figure 4C), as evidenced by the difference spectrum, (D) − (C), in Figure 4F. At pH 5.4, the Zn^{2+} ion does not affect any Raman bands of the peptide main chain, His residues, and Cys residues, indicating that the Zn^{2+} ion does not bind to M1Lnk. This is fully consistent with the CD spectral observation that the secondary structure of M1Lnk is not affected by Zn^{2+} at pH 5.4 (Figures 1 and 2). The Raman spectra clearly show that M1Lnk releases the Zn^{2+} atom and refolds into the α-helical structure upon acidification. The release of Zn^{2+} may be initiated by the protonation of His159 and His162, which is followed by the recovery of the S−H bonds of Cys148 and Cys151 residues. Raman and NMR studies on Cys_2His_2-type Zn fingers have shown that the affinity of His for Zn^{2+} is lower than that of Cys (*42*) and protonation of His residues takes place prior to that of Cys residues upon acidification (*43*). The acid-induced dissociation of Zn^{2+} from M1Lnk is likely to occur in a similar way.

Coordination Geometry of Zn^{2+}-M1Lnk. The Zn^{2+} ion does not show electronic transitions in the visible region, whereas the Co^{2+} ion, which has an ionic radius and polarizability similar to those of Zn^{2+}, exhibits visible absorption due to d-d transition (*44*, *45*). The Co^{2+} d-d absorption band is sensitive to both the ligand composition and geometry of the first coordination shell (*45*, *46*). Thus, the Co^{2+} ion serves as a useful probe of Zn^{2+}−peptide interactions. Absorption spectra of M1Lnk titrated with Co^{2+} at pH 7.4 in 50% TFE solution are shown in Figure 5A. Three transitions at 570, 630, and 665 nm gain intensity with increase of the Co^{2+} concentration, and finally a broad absorption band is formed in the presence of 5 equiv of Co^{2+}. Since the shape of the absorption band does not change during the titration, it is evident that a single coordination species is present throughout the titration. The wavelength and shape of the absorption band in Figure 5A are characteristic of the Co^{2+} ion tetrahedrally coordinated by two sulfur and two nitrogen atoms (*45*, *46*). The absorbance at 665 nm is plotted against the molar ratio of Co^{2+}/M1Lnk in Figure 5B, yielding an apparent dissociation constant K_d of $(3.6 \pm 1.0) \times 10^{-6}$ M.

Back-titration of Co^{2+}−M1Lnk with Zn^{2+} was performed to determine whether Zn^{2+} binds to the same site as Co^{2+} does. As shown in Figure 5C, the Co^{2+} absorption intensity decreases linearly with increase of the Zn^{2+} concentration and almost diminishes in an equimolar mixture of Zn^{2+} and M1Lnk. This observation clearly shows that the Zn^{2+} ion displaces the Co^{2+} ion. The apparent dissociation constant of Zn^{2+}−M1Lnk was calculated to be $K_d = (1.0 \pm 0.5) \times 10^{-9}$ M from the plot of back-titration. The K_d value for Zn^{2+} is much smaller than that for Co^{2+}, being consistent with

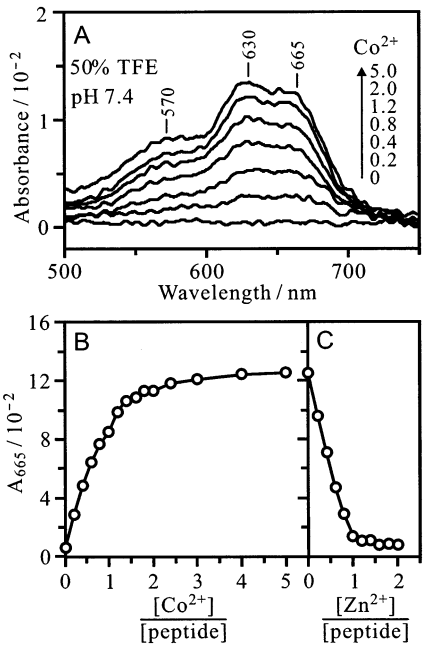

FIGURE 5: (A) Visible absorption spectra of M1Lnk in the absence and presence of Co^{2+} at pH 7.4. The solutions contained 25 μM peptide, 30 mM HEPES (pH 7.4), 100 mM $NaClO_4$, and 50% (v/v) TFE. Varied (0.2−5.0) equivalents of Co^{2+} were added as indicated. (B) Titration of M1Lnk with Co^{2+}. The absorbance at 665 nm (A_{665}) is plotted against the Co^{2+}/peptide molar ratio. (C) Back-titration of M1Lnk with Zn^{2+}. The A_{665} value is plotted against the Zn^{2+}/peptide molar ratio. The Zn^{2+} ion was added to the solution already containing 5 equiv of Co^{2+}. The solution conditions in (B) and (C) are the same as in (A).

the finding that the Zn^{2+} complex is orders of magnitude more stable than its Co^{2+} counterpart in a tetrahedral ligand field composed of two sulfur and two nitrogen atoms (*45*). The CD spectrum recorded for Co^{2+}−M1Lnk at pH 7.4 (not shown) was almost identical to that of Zn^{2+}−M1Lnk in Figure 2, indicating that the displacement of Co^{2+} by Zn^{2+} occurs without significant conformational change of the peptide. Taken together with the results of Raman spectral analysis, it is concluded that the Zn^{2+} ion is tetrahedrally coordinated by the sulfur atoms of Cys148 and Cys151 as well as the imidazole nitrogen atoms (one N_π and the other N_τ) of His159 and His162 at neutral pH.

DISCUSSION

The spectral data obtained here show evidence that M1Lnk binds to a Zn^{2+} ion at neutral pH by using its Cys_2His_2 motif. The side chains of the Cys and His residues are coordinated to the Zn^{2+} ion in a tetrahedral geometry, and the peptide main chain is partially unfolded to facilitate the Zn^{2+} binding. The Zn^{2+}−M1Lnk coordination is disrupted at acidic pH, and the peptide refolds into the original α-helical conformation. The conformation of M1Lnk is sensitive to pH only in the presence of Zn^{2+}, and Zn^{2+}-free M1Lnk remains α-helical at both neutral and acidic pH. Thus, the Cys_2His_2 motif is essential for M1Lnk to obtain the pH sensitivity of the conformation.

Some Zn finger peptides also contain Cys_2His_2 motifs. However, the arrangement of two Cys and two His residues in M1Lnk significantly differs from that of the Cys_2His_2 motif in Zn finger proteins (*47*). A typical Cys_2His_2-type Zn finger protein contain 12 amino acid residues between

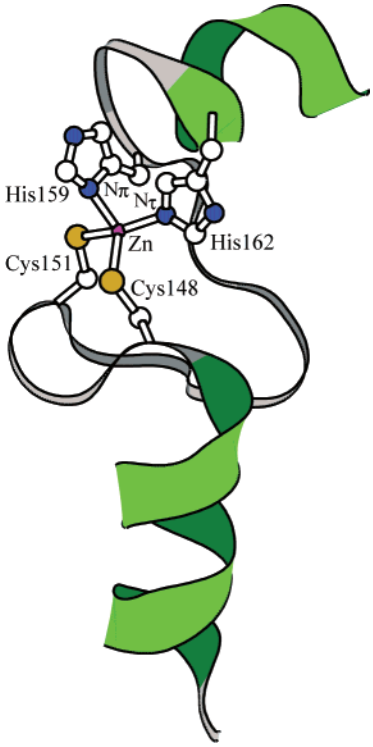

FIGURE 6: Model for Zn^{2+}-bound M1Lnk. Side chains are shown only for the Cys and His residues.

the second Cys residue and the first His residue, whereas M1Lnk contains an insertion of only 7 residues. Two His residues are separated by 3−5 residues in Zn fingers but by only 2 residues in M1Lnk. Binding of Zn^{2+} to the Cys_2His_2-type Zn finger peptide usually induces α-helical conformation in the His-containing region so that two His residues can coordinate to the same Zn^{2+} ion (*48*, *49*). In sharp contrast, the Zn^{2+} binding to M1Lnk induces partial unfolding of the helix as described in the Results section. These differences suggest that the structure of Zn^{2+}-bound M1Lnk is not analogous to that of the Zn finger, which consists of two antiparallel β-strands followed by an α-helix (*47*). The structural difference may be reflected in the sensitivity to acidification. The Zn^{2+} ion dissociates from the Cys_2His_2-type Zn finger at pH 5 (*43*), whereas the Zn^{2+} dissociation from M1Lnk takes place at pH 5.9. The elevated sensitivity of the putative linker region may be useful in detecting the internal pH change of the virion.

A possible model for Zn^{2+}-bound M1Lnk was searched computationally starting from the highly α-helical structure of Zn^{2+}-free M1Lnk based on the X-ray crystal structure at pH 7.4 for residues 139−158 (*26*; PDB code 1EA3) and the standard amino acid geometrical parameters for residues 159−166 (*50*). In the computation, the peptide main-chain $\phi-\psi$ torsion angles and the side chain $\chi^1-\chi^{2,1}$ torsion angles of the Cys and His residues were varied using a Monte Carlo method to find a structure that fulfills the requirement of tetrahedral coordination of the Cys and His ligands to a Zn^{2+} ion. Figure 6 shows a structural model, of which the stereochemical quality was checked by the ProCheck software (*51*). The $\phi-\psi$ and $\chi^1-\chi^{2,1}$ angles obtained are listed in Table 1. In the model, long and short helices are connected with a loop region that binds to a Zn^{2+} ion. The long helix belongs to the N-terminal domain of M1 and the short helix to the C-terminal domain. The α-helical content (46%) of

Table 1: Torsion Angles in a Structural Model for Zn^{2+}-Bound M1Lnk[a]

residue	ϕ	ψ	χ^1	$\chi^{2,1}$
Val147	−49.9	−60.1		
Cys148	−134.9	−44.9	−179.9	
Ala149	93.4	13.2		
Thr150	−164.5	−67.0		
Cys151	−51.5	178.0	−66.0	
Glu152	−87.8	−124.8		
Gln153	−12.8	74.8		
Ile154	−40.8	−68.8		
Ala155	−47.4	−47.7		
Asp156	−135.7	102.7		
Ser157	−131.6	94.9		
Gln158	−57.9	72.5		
His159	−71.3	151.8	174.7	128.1
Arg160	−53.9	−66.3		
Ser161	−67.8	−93.1		
His162	−54.2	−40.1	82.3	129.9
Arg163	−61.9	−40.9		
Gln164	−62.2	−40.7		
Met165	−61.9	−41.0		
Val166	−61.9			

[a] Main-chain (ϕ and ψ) and side-chain (χ^1 and $\chi^{2,1}$) torsional angles varied in Monte Carlo calculations. The values are given in degrees. The other geometrical parameters for residues 139−158 were assumed to be the same as in the X-ray crystal structure of the Zn-free N-terminal fragment of M1 (*26*; PDB code 1EA3). For residues 159−166, X-ray diffraction data are not available, and the geometrical parameters were taken from those proposed by Momany et al. (*50*). In the model, the Zn^{2+} ion is located at a distance of 2.27−2.29 Å from the sulfur atoms of Cys148 and Cys151 and at a distance of 1.93−1.98 Å from the nitrogen atoms of His159 and His162.

the model is consistent with that (50%) estimated from CD spectra, and the pair of ligand nitrogen atoms of His residues (N_π and N_τ) is also consistent with the finding by Raman spectroscopy. The model in Figure 6 may represent a plausible structure of Zn^{2+}-bound M1Lnk.

The influenza A virus contains a small but significant number of Zn ions (*30*), though the crystals of the N-terminal fragment examined by X-ray diffraction did not contain Zn ions (*25*−*27*). The Zn ions in the virion are tightly bound to about 10% of the M1 molecules (*30*). The Zn−M1 tight binding is consistent with a very small dissociation constant (1.0×10^{-9} M) of Zn^{2+}−M1Lnk. It is likely that some M1 molecules are bound to a Zn^{2+} ion via two Cys and two His side chains in a tetrahedral geometry as seen for the Zn^{2+}−M1Lnk complex. In the absence of Zn^{2+}, helix H9 is surrounded by the other four helices as revealed by X-ray diffraction (*25*−*27*). Cys148 and Cys151 located on the same side of helix H9 are not buried within the domain but accessible from the domain surface. Thus, the Cys residues can coordinate to a Zn^{2+} ion if helix H9 is partially unfolded. His159 and His161 on the C-terminal side of helix H9 are also accessible to the Zn^{2+} ion. Thus, the tetrahedral coordination of the Cys_2His_2 motif to a Zn^{2+} ion can be achieved without destruction of the domain structure. The putative linker region of Zn^{2+}-bound M1 is likely to take a structure similar to that shown in Figure 6 for Zn^{2+}−M1Lnk. It is also plausible that the Zn^{2+} ion is released from the Cys_2His_2 motif at acidic pH and the M1 linker region retains α-helical structure as in the case of M1Lnk. The transition from the partially unfolded Zn^{2+}-bound conformation at neutral pH to the highly α-helical Zn^{2+}-free conformation at acidic pH would affect the disposition of the N- and C-terminal domains, resulting in an altered interaction between M1 and other viral components. Although Zn^{2+}-bound M1 molecules are not abundant in the virion, they may play a special role in virus uncoating by using their unique sensitivity to acidification.

REFERENCES

1. Lamb, R. A., and Choppin, P. W. (1983) *Annu. Rev. Biochem. 52*, 467−506.
2. White, J. M., Hoffman, L. R., Arevalo, J. H., and Wilson, I. A. (1997) in *Structural Biology of Viruses* (Chiu, W., Burnett, R. M., and Garcea, R. L., Eds.) pp 80−104, Oxford University Press, Cambridge.
3. Portela A., and Digard, P. (2002) *J. Gen. Virol. 83*, 723−734.
4. Lamb, R. A., and Krug, R. M. (1996) in *Fields Virology* (Fields, B. N., Knipe, D. M., and Howley, P. M., Eds.) 3rd ed., pp 1353−1395, Lippincott-Raven, Philadelphia.
5. Ye, Z., Liu, T., Offringa, D. P., McInnis, J., and Levandowski, R. A. (1999) *J. Virol. 73*, 7467−7473.
6. Ruigrok, R. W. H., Barge, A., Durrer, P., Brunner, J., Ma, K., and Whittaker, G. R. (2000) *Virology 267*, 289−298.
7. Ali, A., Avalos, R. T., Ponimaskin, E., and Nayak, D. P. (2000) *J. Virol. 74*, 8709−8719.
8. Zhang, J., and Lamb, R. A. (1996) *Virology 225*, 255−266.
9. Enami, M., and Enami, K. (1996) *J. Virol. 70*, 6653−6657.
10. Carr, C. M., and Kim, P. S. (1993) *Cell 73*, 823−832.
11. Čiampor, F., Cmarko, D., Cmarková, J., and Závodská, E. (1995) *Acta Virol. 39*, 171−181.
12. Pinto, L. H., Dieckmann, G. R., Gandhi, C. S., Papworth, C. G., Braman, J., Shaughnessy, M. A., Lear, J. D., Lamb, R. A., and DeGrado, W. F. (1997) *Proc. Natl. Acad. Sci. U.S.A. 94*, 11301−11306.
13. Okada, A., Miura, T., and Takeuchi, H. (2001) *Biochemistry 40*, 6053−6060.
14. Zhirnov, O. P. (1990) *Virology 176*, 274−279.
15. Bui, M., Whittaker, G., and Helenius, A. (1996) *J. Virol. 70*, 8391−8401.
16. Zoueva, O. P., Bailly, J. E., Nicholls, R., and Brown, E. G. (2002) *Virus Res. 85*, 141−149.
17. O'Neill, R. E., Jaskunas, R., Blobel, G., Palese, P., and Moroianu, J. (1995) *J. Biol. Chem. 270*, 22701−22704.
18. Whittaker, G., Bui, M., and Helenius, A. (1996) *J. Virol. 70*, 2743−2756.
19. Martin, K., and Helenius, A. (1991) *Cell 67*, 117−130.
20. Bui, M., Wills, E. G., Helenius, A., and Whittaker, G. R. (2000) *J. Virol. 74*, 1781−1786.
21. Gómez-Puertas, P., Albo, C., Pérez-Pastrana, E., Vivo, A., and Portela, A. (2000) *J. Virol. 74*, 11538−11547.
22. Barman, S., Ali, A., Hui, E. K.-W., Adhikary, L., and Nayak, D. P. (2001) *Virus Res. 77*, 61−69.
23. Winter, G., and Fields, S. (1980) *Nucleic Acids Res. 8*, 1965−1974.
24. Lamb, R. A., and Lai, C.-J. (1981) *Virology 112*, 746−751.
25. Sha, B., and Luo, M. (1997) *Nat. Struct. Biol. 4*, 239−244.
26. Arzt, S., Baudin, F., Barge, A., Timmins, P., Burmeister, W. P., and Ruigrok, R. W. H. (2001) *Virology 279*, 439−446.
27. Harris, A., Forouhar, F., Qiu, S., Sha, B., and Luo, M. (2001) *Virology 289*, 34−44.
28. Shishkov, A. V., Goldanskii, V. I., Baratova, L. A., Fedorova, N. V., Ksenofontov, A. L., Zhirnov, O. P., and Galkin A. V. (1999) *Proc. Natl. Acd. Sci. U.S.A. 96*, 7827−7830.
29. Wakefield, L., and Brownlee, G. G. (1989) *Nucleic Acids Res. 17*, 8569−8580.
30. Elster, C., Fourest, E., Baudin, F., Larsen, K., Cusack, S., and Ruigrok, R. W. H. (1994) *J. Gen. Virol. 75*, 37−42.
31. Bohm, G., Muhr, R., and Jaenicke, R. (1992) *Protein Eng. 5*, 191−195.
32. Johnson, W. C., Jr. (1988) *Annu. Rev. Biophys. Biophys. Chem. 17*, 145−166.
33. Sönnichsen, F. D., Van Eyk, J. E., Hodges, R. S., and Sykes, B. D. (1992) *Biochemistry 31*, 8790−8798.
34. Shiraki, K., Nishikawa, K., and Goto, Y. (1995) *J. Mol. Biol. 245*, 180−194.
35. Hill, A. V. (1910) *J. Physiol. (London) 40*, 4−7.
36. Fersht, A. (1977) *Enzyme Structure and Mechanism*, Freeman, New York.

37. Harada, I., and Takeuchi, H. (1986) in *Spectroscopy of Biological Systems* (Clark, R. J. H., and Hester, R. E., Eds.) pp 113−175, John Wiley and Sons, New York.
38. Miura, T., Satoh, T., Hori-i, A., and Takeuchi, H. (1998) *J. Raman Spectrosc. 29*, 41−47.
39. Miura, T., Hori-i, A., Mototani, H., and Takeuchi, H. (1999) *Biochemistry 38*, 11560−11569.
40. Li, H., and Thomas, G. J., Jr. (1991) *J. Am. Chem. Soc. 113*, 456−462.
41. Caswell, D. S., and Spiro, T. G. (1986) *J. Am. Chem. Soc. 108*, 6470−6477.
42. Miura, T., Satoh, T., and Takeuchi, H. (1998) *Biochim. Biophys. Acta 1384*, 171−179.
43. Krizek, B. A., Amann, B. T., Kilfoil, V. J., Merkle, D. L., and Berg, J. M. (1991) *J. Am. Chem. Soc. 113*, 4518−4523.
44. Gray, H. B. (1980) *Adv. Inorg. Biochem. 2*, 1−25.
45. Maret, W., and Vallee, B. L. (1993) *Methods Enzymol. 226*, 52−71.
46. Shi, Y., Beger, R. D., and Berg, J. M. (1993) *Biophys. J. 64*, 749−753.
47. Berg, J. M., and Shi, Y. (1996) *Science 271*, 1081−1085.
48. Párraga, G., Horvath, S. J., Eisen, A., Taylor, W. E., Hood, L., Young, E. T., and Klevit, R. E. (1988) *Science 241*, 1489−1492.
49. Lachenmann, M. J., Ladbury, J. E., Phillips, N. B., Narayana, N., Qian, X., and Weiss, M. A. (2002) *J. Mol. Biol. 316*, 969−989.
50. Momany, F. A., McGuire, R. F., Burgess, A. W., and Scheraga, H. A. (1975) *J. Phys. Chem. 79*, 2361−2381.
51. Laskowski, R. A., MacArthur, M. W., Moss, D. S., and Thornton, J. M. (1993) *J. Appl. Crystallogr. 26*, 283−291.

BI027176T